

# Experiments in Second Order Sliding Mode Control of a CPG based Spherical Robot <sup>\*</sup>

Abhra Roy Chowdhury<sup>\*</sup> G. S. Soh<sup>\*</sup> S. H. Foong<sup>\*</sup>  
K. L. Wood<sup>\*\*</sup>

<sup>\*</sup> Temasek Laboratories, Engineering Product Development Pillar,  
Singapore University of Technology and Design, Singapore 487372  
(Email: abhra\_rc@sutd.edu.sg)

<sup>\*\*</sup> SUTD-MIT International Design Centre, Singapore University of  
Technology and Design, Singapore 487372

---

**Abstract:** A novel caterpillar inspired rolling gait generation in a spherical robot and its control mechanism is presented in this paper. A rhythmic rolling pattern mimicking Pleurotya caterpillar is produced for the spherical robot locomotion. The pattern is represented by central pattern generators (*CPGs*) in combination with nonlinear robot dynamics. These rhythmic patterns are controlled by a non-linear high (second) order sliding mode (*HOSMC*) feedback method, to maintain robot stability and robustness in the presence of matched parameter uncertainties and bounded external disturbances. Design and experimental evaluation of the proposed control strategy for the spherical robot is done on both smooth and rough ground surfaces. Control performance of the robot is measured by virtue of roll angle stability, its convergence and wheel velocities. Experimental results validate that proposed second-order *HOSMC* strategy is more efficient in robust rolling gait control of a spherical robot compared to a first-order *SMC* on two different types of ground surfaces.

Keywords: Pleurotya caterpillar, Bioinspiration, Spherical Robot, Central Pattern Generator (*CPG*), Rolling gait, Rolling friction, High order sliding mode (*HOSMC*) Control.

---

## 1. INTRODUCTION

Active rolling locomotion [1] is a fascinating insect behaviour where the organism uses its own energy to roll and control its direction simultaneously. Some examples portraying active rolling are Pleurotya (Mother-of-pearl moth) caterpillar [2,3], Stomatopod shrimp, Huntsman spider etc. During a predator attack [3,4], these invertebrate insects recoil themselves into a wheel shape with heads pushed inside while back to outside. This results into swift and efficient rolling action over a considerable distance to evade the danger. Reports indicate a rolling speed forty times more compared to the normal crawling speed in the case of a Pleurotya caterpillar. The two distinctive advantages of speed and efficiency are exploited by these invertebrates locomotion by using recoil-roll mechanism [4]. Study of rolling gaits is an intriguing feature of rolling mechanism found in invertebrates [4]. It is assumed that a series of discrete and faster rolling gait impulses add up to produce one-sided complete continuous rolling motion of caterpillar denoted by angular parameter  $\beta_1$ . Section 2 discusses the parameter  $\beta$ . The biological term referred to generating coordinated rhythmic patterns in both crawling vertebrates and insect invertebrates, is known as central pattern generators (*CPG*) [5]. Bionics (robots)[5,6,7] have extensively used *CPG* network and dynamics. *CPG* net-

work can support distributed control structure, inherent stability of a limit cycle, global convergence and time delay reduction. These control properties are utilized to modulate(tune) body parameters and integrate sensory feedback capability [8,24] in mobile robots. Present research is aimed to understand and exploit these benefits by mimicking caterpillar active rolling patterns in a spherical robot as shown in Fig.1. Caterpillar inspired rolling gait for the spherical robot is obtained from an asymmetric nonlinear oscillator [9] based mathematical model. Details are presented in section 3. Recent times have witnessed the emergence and utility of research in spherical robots [10,11,12]. During a collision with obstacles, a roll-over is avoided due to its symmetrical, non-invertible structure. A noteworthy contributor towards its energy efficiency is the single point of contact of robot outer shell with the ground. The spherical rolling robots are suited for dynamic or irregular terrains due to their ability to withstand irregularities. For instance, rolling-down action from the dynes or slopes can leverage considerable onboard energy savings. Another agility feature is omnidirectional driving. During obstacle interaction, swiftly changing its direction without retracting from earlier path contributes significantly to overall time and effort. In contrast to the earlier research that uses fixed-pattern rolling trajectory waveforms, present research proposes a non-linear oscillator based *CPG* network to spawn different kinds of coordinated rolling gait patterns of the spherical robot.

---

<sup>\*</sup> This work is supported by the Future Systems and Technology Directorate (FSTD), under the Ministry of Defense, Government of Singapore, under Grant IGDST1301013 for Systems Technology for Autonomous Reconnaissance and Surveillance (STARS) project.

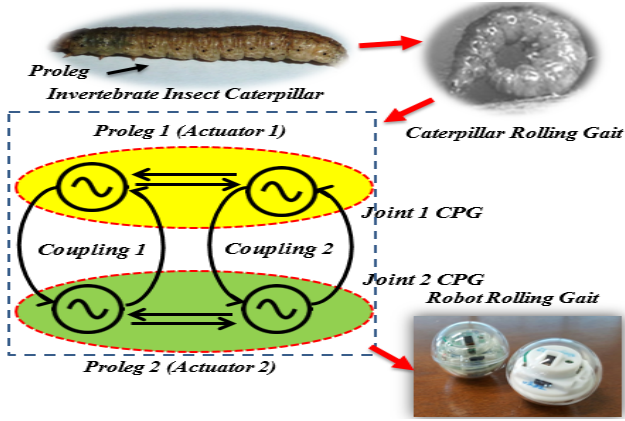


Fig. 1. Caterpillar rolling gait pattern generated by coupled motoneuron actuates spherical robot

Design and development of a robust control system [12,14] of spherical robot is found to be the research intensive focus in many reports. Present paper further integrates it to the rolling gait based driving mechanics. Many researchers have proposed various designs ranging from classic *LQR* [13], nonlinear robust [12,16,19] and optimal [20] methods to control the robot smoothly through its environment. A trajectory tracking control of spherical robot on straight paths has been investigated successfully using various schemes like adaptive hierarchical sliding mode (*HSMC*) [16] and high order sliding mode control [21,22] methods. Recently, researchers [17] have proposed a combined adaptive neuro-fuzzy and *SMC* method to regulate robot trajectory. According to literature, dynamical model based first-order sliding mode control *SMC* [13,14] method emerges out to be a preferred strategy adopted by most researchers. This strategy ensures fast robust dynamic response under parameter uncertainties, unmodeled dynamics and bounded disturbances. However, the evaluation of the traditional (first-order) *SMC* method has shown major drawbacks such as chattering effect, limited flexibility of sliding function design etc. One of the approaches to address these limitations is by introducing a higher-order sliding mode *HOSMC*. In contrast to the first-order *SMC*, proposed high (second)-order *HOSMC* reduces chattering, provides a smooth control and better convergence accuracy while preserving the robustness properties. Therefore, it offers better performance, stability and less energy loss of the system.

Previously researchers have presented a comprehensive theoretical work on *HOSMC* method of robot control mainly through simulation in ideal conditions. So, it is vital to discuss experimental evaluation of these control algorithms in real time under uncertainties and bounded disturbances. Therefore, motivated from these facts, the following contributions of present research are enumerated below:

- Develop and implement a caterpillar-rolling gait [4] inspired asymmetrical *CPG* model in a spherical robot rolling locomotion.
- Develop the spherical robot non-linear dynamics inclusive of actuator dynamics and rolling resistance (friction) [15].

- Define a novel feedback control architecture of the robot integrated with its non-linear dynamics. The coordinated pattern output generates desired rolling gait trajectory. A feedback policy based on second order sliding mode control (*HOSMC*) delivers robustness to rolling motion against external disturbances and parameter uncertainties.
- Evaluate and compare the proposed second-order *HOSMC* control strategy against traditional first-order *SMC* through "experiments" in both smooth plane (indoor environment) and irregular rough (outdoor environment) surfaces.
- Demonstrate the feasibility of a real-time spherical robot prototype propelled by a bioinspired active rolling gait and a unique control architecture.

Rest of the paper is organized as follows. In section 2, the system modeling of spherical robot is presented. Contribution of different body parameters are discussed in the perspective of rolling mode dynamics. Actuator and rolling friction models have been integrated in overall robot dynamics. Section 3 elaborates *HOSMC* based feedback control strategy. Subsection 1 formulates a trajectory generator based on caterpillar-rolling gait based *CPG* model. Subsequently, in subsection 2, a nonlinear second-order *HOSMC* control strategy is employed to add robustness to the resulting rolling motion of robot. In section 4, the implementation of this control algorithm is discussed and verified under two different ground conditions i.e. plane surface and rough surface. Results are further evaluated and compared with the experimental results of a first-order *SMC* technique. In Section 5, conclusions and directions of future work are presented.

## 2. SYSTEM MODEL

Spherical robot comprises of an inner differential-drive cart and an outer spherical shell. Planar rolling motion of robot is achieved by moving away its center of mass (*COM*) through its neutral equilibrium position. The complex robot non-linear model is decoupled [12] into two typical motion modes: rolling and spinning. The decoupled approach simplifies controller implementation of its complex kinematics and dynamics model. It is assumed that there is no slip between shell and floor as well as between drive wheels and shell.

### 2.1 Rolling Mode

A pure rolling motion is considered with identical drive wheel speeds. Side view of robot is shown Fig.2. A local frame  $\{S\}$  parallel to the world frame  $\{W\}$  is fixed on shell center and another local frame  $\{C\}$  on cart mass center. With non-slip assumption as observed in  $\{S\}$ , relative motion at contact point between cart wheel and shell is absent, i.e.,

$$w_x r_i = \dot{\beta} r_i + \dot{\theta} r_w \quad (1)$$

where  $w_x$  is shell angular velocity around the  $x$ -axis of  $\{S\}$ ,  $\beta$  is cart roll angle,  $\theta$  is wheel angle in  $\{C\}$ ,  $r_i$  is distance from shell center to contact point,  $r_s$  is shell radius, and  $r_w$  is radius of cart wheel. It is shown to be influenced by cart roll motion and wheel rotation. The sphere center velocity is given by

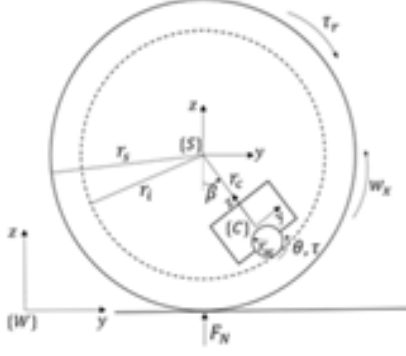


Fig. 2. System model showing the spherical robot parameters

$$\mathbf{v}_s = \begin{pmatrix} \dot{x} \\ \dot{y} \\ \dot{z} \end{pmatrix} = \begin{pmatrix} 0 \\ -r_s w_x \\ 0 \end{pmatrix} \quad (2)$$

Kinetic energy of shell is derived as

$$T_s = \frac{1}{2} m_s \|\mathbf{v}_s\|^2 + \frac{1}{2} I_s w_x^2 \quad (3)$$

where  $m_s$  represents shell mass and  $I_s$  is shell inertia.

Further, velocity of cart mass center is given by

$$\mathbf{v}_c = \mathbf{v}_s + r_c \dot{\beta} \begin{pmatrix} 0 \\ \cos \beta \\ \sin \beta \end{pmatrix} = \begin{pmatrix} 0 \\ r_c \dot{\beta} \cos \beta - r_s w_x \\ r_c \dot{\beta} \sin \beta \end{pmatrix} \quad (4)$$

Kinetic energy of cart is given by

$$T_c = \frac{1}{2} m_c \|\mathbf{v}_c\|^2 + \frac{1}{2} I_c \dot{\beta}^2 + I_w (\dot{\beta} + \dot{\theta})^2 \quad (5)$$

where  $m_c$  is cart mass,  $I_c$  is cart inertia around  $x$ -axis of  $\{C\}$ , and  $I_w$  is wheel inertia w.r.t. rotational axis. The potential energy of shell is constant as it rolls on flat surface. Potential energy of the cart is given by

$$V_c = m_c g (r_s - r_c \cos \beta) \quad (6)$$

where  $g = -9.8$  m/sec<sup>2</sup>.

The net torque  $\tau_m$  generated from motor output is the external (actuator) force acting on robot. In addition, there is rolling friction [15] acting on robot to oppose its motion, denoted as resisting torque  $\tau_r$  exerting negative work on the robot. Uncertainty due to noise disturbance  $\delta q$  has been assumed to be a time invariant fraction. Therefore, virtual work done by these external forces is formulated by

$$\begin{aligned} \delta W &= -\tau_r w_x \delta t + \tau_m \delta \theta + \delta q \\ &= -\tau_r \left( \delta \beta + \frac{r_w}{r_i} \delta \theta \right) + \tau_m \delta \theta + \delta q \\ &= -\tau_r \delta \beta + \left( \tau_m - \tau_r \frac{r_w}{r_i} \right) \delta \theta + \delta q \end{aligned} \quad (7)$$

The inertia forces and torques defined for the system are given by:

$$\text{Reaction Force : } R_i = -m_{sc}^0 a_i \quad (8)$$

$$\text{Torque : } T_i = -{}^0 I_{sc}^0 \alpha_i - {}^0 w_{xi} \times {}^0 I_{sc}^0 w_{xi} \quad (9)$$

where

$$m_{sc} = m_s + m_c \quad (10)$$

$a_i$  and  $\alpha_i$  is linear and angular acceleration of robot respectively. According to the *Euler-Lagrange* equation, we have

$$\begin{aligned} M \begin{pmatrix} \ddot{\beta} \\ \ddot{\theta} \end{pmatrix} + m_c r_c r_s \dot{\beta}^2 \sin \beta \begin{pmatrix} 1 \\ \frac{r_w}{r_i} \end{pmatrix} \\ + \begin{pmatrix} m_c r_c g \sin \beta \\ 0 \end{pmatrix} &= \begin{pmatrix} -\tau_r \\ \tau_1 - \tau_r \frac{r_w}{r_i} \end{pmatrix} \end{aligned} \quad (11)$$

where

$$M = \begin{pmatrix} M_{11} & M_{12} \\ M_{21} & M_{22} \end{pmatrix}$$

$$M_{11}(\beta) = m_{sc} r_s^2 + m_c r_c^2 + I_s + I_c - 2m_c r_c r_s \cos \beta$$

$$M_{12}(\beta) = M_{21} = (m_{sc} r_s^2 + I_s) \frac{r_w}{r_i} + 2I_w - m_c r_c r_s \frac{r_w}{r_i} \cos \beta$$

$$M_{22} = (m_{sc} r_s^2 + I_s) \left( \frac{r_w}{r_i} \right)^2 + 2I_w \quad (12)$$

Roll angle  $\beta$  majorly influences rolling stability. It in-turn relies on wheel angular acceleration  $\ddot{\theta}$  produced by  $M_{12}$ . Value of  $M_{12}$  is directly proportional to wheel radius and wheel inertia. Wheel angular acceleration is desired to have less impact on roll angle dynamics, in order to obtain stable motion of robot. However, in the presence of external (bounded) disturbance and model uncertainties, a robust control strategy is required to stabilize  $\beta$ .

### 2.1.1 Control forces and Servo motor Actuator Dynamics

Present robot system uses two geared dc motor actuators. They are utilized as control inputs to provide planar forward and turning motion. In a *DC* motor equation with standard notation, torque  $\tau_i$  is a function of angular rotational velocity  $\omega_m$  and armature voltage  $v_a$  given by

$$\tau_i = f(\omega_m, v_a) \quad (13)$$

where armature voltage  $v_a$  is

$$v_a = \frac{r_a}{K_m} \tau_m + K_e \dot{\theta}_m \quad (14)$$

$\tau_m$  is the motor torque then  $\tau_i$  can be written as

$$\tau_i = f(\omega_m, \tau_m) \quad (15)$$

The generalized active control force is expressed as

$$\tau_m = \frac{\partial^0 \omega_i}{\partial \theta_t} \cdot T_0 + \frac{\partial^0 v_i}{\partial \theta_t} \cdot R_0 + \sum_{i=1}^2 \left( \frac{\partial^0 \omega_i}{\partial \theta_t} \cdot \tau_i \right) \quad (16)$$

**2.1.2 Rolling Resistance** Eluding slip between driving wheel and shell surface, spherical robot has to possess a certain amount of rolling resistance (friction)[15] during rolling. Rolling resistance model is assimilated to characterize resistive forces and moments acting on spherical rolling robot at equilibrium. Interaction between robot external shell and wheel's floor interface is depicted by this model. Resultant force from this rolling resistance being centred at wheel's origin, directs parallel to the angular velocity. However, resultant torque arising from re-distribution of normal forces oppose this characteristic of rolling resistance. Therefore, a net decelerating motion of robot can be observed.

Empirically, rolling resistance force is formulated as

$$\tau_f = \frac{\mu}{r_s} \cdot (N) \quad (17)$$

where  $\mu$  is the coefficient of rolling resistance.

Rolling resistance torque is governed by equation

$$\tau_m = r_s \times N = 0.15 \sqrt{\frac{R}{l \cdot E}} \cdot (N)^{3/2} \quad (18)$$

where,  $r_s$  is shell radius,  $N$  is normal force,  $l$  is length of rectangular contact surface patch and  $E$  is reduced elasticity (considering both contact surfaces to be non-rigid). Therefore, the generalized rolling resistance force is given by combining ,

$$\tau_r = \tau_f + \tau_m \quad (19)$$

Above quasi-static model is found to show reliable behaviour [15] in depressing environments.

### 3. CONTROLLER DESIGN

Proposed control law is a unique strategy developed and implemented for a spherical robot to the best of our knowledge. As shown in Fig.3, the rhythmic rotational motion of driving wheels is regulated by a feedback policy. The output of the trajectory generator is the rolling gait *CPG* signal. These controllable and stable rhythmic patterns are responsible to drive robot actuators similar to its biological counterpart, the central pattern generators in actual caterpillar locomotion [3,4]. Being in a dynamic environment, a nonlinear high-order (second-order) sliding mode control [21,22] method is introduced to reinforce the *CPG* gait control by providing a robust and smooth response in the presence of external disturbances and uncertain parameters.

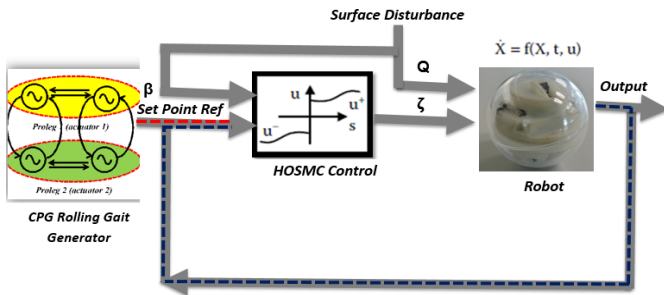


Fig. 3. Block diagram of feedback nonlinear control scheme

#### 3.1 Rolling gait generator

Coordinated locomotion patterns or gaits are displayed by invertebrates like *Pleurotya* caterpillars [2,4]. These are represented by a distributed network of neurons termed as pattern generator. Central pattern generator (*CPG*) [5] based neuronal coordination is widely used in bio-inspired robot locomotion [6,7,24]. Coupled non-linear oscillators possess stability characteristics of self-sustained limit cycle behavior [18]. It is useful in mitigating transient perturbations in distressed environment. Numerical modeling of *CPG* architecture presented in this research originates from a *Matsuoka* based coupled non-linear oscillator [9,18]. The output of coupled non-linear oscillator defines the rolling gait (stable roll angle  $\beta$ ) for spherical robot locomotion. It consists of two asymmetric nonlinear oscillators

coupled together with kinematic parameters and tuned coupling gains. A set of differential equations governing the non-linear dynamical system is represented by

$$\frac{\partial p_1}{\partial t} = -p_1 + \eta q_1 - \zeta q_2 + f(t)_{s1} \quad (20)$$

$$\frac{\partial p_2}{\partial t} = -p_2 + \eta q_1 + \zeta q_2 + f(t)_{s2} \quad (21)$$

where neuron firing rate and neuron output is given by  $p_i$  and  $q_i$  respectively, self-inhibition is denoted by adaption constant  $\zeta$  and  $\eta$  regulates mutual inhibition. Periodic input to the oscillator is  $f(t)_{si}$ . *Matsuoka* oscillator based entrainment techniques have been used to control humanoid robots with robustness and reliability. Distinct non-linear oscillator models [8,9,24] have been used to impart adaptation behaviour in robot applications. These behaviours are inspired by a group of biological interconnected neurons. *CPG*'s are often modeled as coupled dynamical oscillators which have stability characteristics of self-sustained limit cycle behavior by suppressing transient perturbations. A pair of mutually coupled asymmetric oscillators can be expressed as

$$\dot{y}_i(\beta) = h(y_i) + k \sum_j w_{ij} [g_{ij} S(\alpha_{ij})(y_j - c_j) - (y_i - c_i)] + q(y_i) \quad (22)$$

where oscillator index numbers are given by  $i$  and  $j$ , oscillator  $i$  and oscillator  $j$  are directly inter-connected.  $h(y_i)$  shows a self-response of neuron function  $y$ . In this case, oscillator output corresponds to roll angle ( $\beta$ ). Subsequent term represents mutual response to other connected oscillators.  $k$  is coupling constant,  $c_i$  is nodal centre,  $w_{ij}$  denotes weight of connecting oscillators,  $g_{ij}$  is amplitude ratio,  $\alpha_{ij}$  is phase difference. Topology dimension is measured by  $S$ , a rotation matrix given by

$$\begin{pmatrix} \cos \alpha_{ij} & \sin \alpha_{ij} \\ \sin \alpha_{ij} & \cos \alpha_{ij} \end{pmatrix} \quad (23)$$

One dimensional topology [ $S = 1$ ] for oscillator arrangement has been used in present model to reduce computational intensity.  $q(y_i)$  adds neuronal response of external disturbance (rolling friction and noise). Resulting rhythmic rolling gait ( $\beta$ ) waveform can be seen in Fig.4(a). Resulting rolling gait *CPG* trajectory is coupled to spherical robot dynamics. It generates a stable and sustained limit cycle as observed in illustrated in Fig.4(b). The limit cycle property also implies desired coordination between the controller, kinematic and dynamic framework of robot. Therefore, two different rolling gait trajectories are generated. A smooth ground surface gait is illustrated in Fig.4(c) with corresponding value of  $q(y_i)$  to be zero whereas a rough (irregular) ground surface gait is shown in Fig.4(d) adopting a higher  $q(y_i)$  value for the resulting rolling gait equation. A non-linear stability analysis of limit cycle behaviour [18] is done using the describing function method. A sinusoidal input is considered as  $f(t)_s$  to be comprised of amplitude  $a_{si}$ , frequency  $\omega_{si}$  and phase  $\phi_{si}$

$$f(t)_{si} = a_{si} \sin(\omega_{si}t + \phi_{si}) \quad (24)$$

Using harmonic balance method, the output of non-linear component  $y(t)_s$  is expressed as

$$y(t)_s \approx a_1 \sin(\omega_{s1}t + \phi_{s1}) + b_1 \sin(\omega_{s2}t + \phi_{s2}) = M \sin(\omega_s t + \phi_s) \quad (25)$$

where

$$a_1 = \frac{1}{\pi} \int_{-\pi}^{\pi} c(t) \cos(\omega t + \phi) d(\omega t) \quad (26)$$

$$b_1 = \frac{1}{\pi} \int_{-\pi}^{\pi} c(t) \sin(\omega t + \phi) d(\omega t) \quad (27)$$

with magnitude and phase are given by

$$M = (a_1^2 + b_1^2)^{1/2} \quad (28)$$

$$\phi = \arctan(a_1, b_1) \quad (29)$$

Non-linear frequency response or describing function  $H(a_{si}, \omega_{si})$  is defined as the complex ratio of fundamental component of input  $f(t)_s$  and output signal  $y(t)_s$

$$H(a_{si}, \omega_{si}) = \frac{M \exp^{j(\omega t + \phi)}}{a \exp^{j(\omega t)}} \quad (30)$$

Fundamental component of  $i/p$  and  $o/p$  must have a phase lag of  $\pi$  to construct a stable limit cycle behaviour.

$$\arg Y(j\omega) = -\pi \quad (31)$$

which can be represented as

$$Y(j\omega)H(a_{si}, \omega_{si}) = -1 \quad (32)$$

$$Y(j\omega) = \frac{-1}{H(a_{si}, \omega_{si})} \quad (33)$$

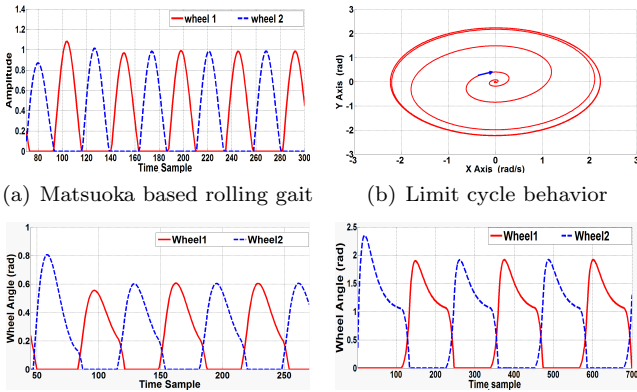


Fig. 4. CPG rolling gait and generated trajectory wrt parameter  $\beta$

### 3.2 Second Order Sliding Mode Feedback Controller

Stability and robustness are considered to be the most desired prospects for underactuated systems like spherical robots [12,19,20]. These indicate system's regulated and steady response towards inaccurate inputs or complex environmental conditions. To deal with this problem, an improved nonlinear sliding control method known as high-order(second-order) sliding mode control (*HOSMC*) [21,22], is implemented as a feedback control strategy for the present robot, to demonstrate applicability of the proposed control. It also shown to serve as a more useful alternative control to traditional first-order *SMC*

control [12,14]. In contrast to the first-order, the second-order (higher-order) input operates on second(higher) derivatives of sliding surface. Its control implementation results in attenuating chattering attenuation, improved convergence accuracy and robust handling of uncertain parameters. In second-order *SMC* (as a particular case of *HOSMC*), the approach is to steer the state (error) towards the switching surface while keeping its sliding surface and its first-order time derivative to be a null vector. A *PID* sliding surface [21] with two independent gains is designed to obtain a second-order sliding mode and executed on a practical spherical robot. It helps to match the system dimension with that of state space. With the help of it, system trajectory is able reach a definite control point from a sliding surface in the multi-dimensional space. Therefore, system robustness is preserved in the entire state space under uncertainties and bounded disturbances. Spherical robot dynamic model with unmatched uncertainties and external disturbance in state space is formulated below. Parametric uncertainty study is done for the roll angle  $\beta$ . Rolling resistance (friction) and noise are treated as external (bounded) disturbance. Then rolling dynamics is rearranged as

$$\ddot{x} = A(x) + B(x)\tau_{fb} + Q(x, \tau) \quad (34)$$

where

$$x = \begin{pmatrix} \beta \\ \theta \end{pmatrix} \quad (35)$$

$$A(x) = -M^{-1} \begin{pmatrix} m_c r_c r_s \dot{\beta}^2 \sin \beta + m_c r_c g \sin \beta \\ \frac{r_w}{r_i} m_c r_c r_s \dot{\beta}^2 \sin \beta \end{pmatrix} \quad (36)$$

$$B(x) = \frac{1}{|M|} \begin{pmatrix} -M_{12} \\ M_{11} \end{pmatrix} \quad (37)$$

Bounded (external) disturbance and parameter uncertainty together is represented by

$$Q(\beta, \tau) = [q_1(\beta, \tau), q_2(\beta, \tau)] \quad (38)$$

Here,

$$\begin{aligned} q_1(\beta, \tau) &= \Delta A_1(\beta) + \Delta B_1(\beta)\tau + w_1 \\ q_2(\beta, \tau) &= \Delta A_2(\beta) + \Delta B_2(\beta)\tau + w_2 \end{aligned} \quad (39)$$

$w$  is the external noise. In the case when only wheel speed rather than motor torque is tunable, wheel angular acceleration is considered as the virtual control input. Rolling dynamics is modified as

$$\begin{pmatrix} \ddot{\beta} \\ \ddot{\theta} \end{pmatrix} = \underbrace{\begin{pmatrix} -M_{11}^{-1} (m_c r_c r_s \dot{\beta}^2 \sin \beta + m_c r_c g \sin \beta) \\ 0 \end{pmatrix}}_{\mathbb{A}} + \underbrace{\begin{pmatrix} -M_{11}^{-1} M_{12} \\ 1 \end{pmatrix}}_{\mathbb{B}} \tau \quad (40)$$

Control objective is to design the input  $\tau$  so that  $x$  tracks its reference  $x_r$ . Tracking error is defined as

$$\tilde{x} = x - x_r \quad (41)$$

a *PID* type sliding surface variable is given below

$$s = \lambda^T \dot{\tilde{x}} + \mu^T \tilde{x} + \nu^T \int_0^t \tilde{x}(t) dt \quad (42)$$

where  $\lambda, \mu, \nu \in \mathfrak{R}^+$  are chosen to be positive definite matrices. Differentiating sliding variable (42) gives

$$\dot{s} = \lambda^T \ddot{\tilde{x}} + \mu^T \dot{\tilde{x}} + \nu^T \tilde{x} \quad (43)$$

$$\dot{s} = \lambda^T (\mathbb{A} + \mathbb{B}\tau + \mathbb{Q}) - \ddot{x}_r + \mu^T \dot{\tilde{x}} + \nu^T \tilde{x} \quad (44)$$

Differentiating the derivative of  $s$  (42) wrt time gives

$$\ddot{s} = \lambda^T (\mathbb{A} + \mathbb{B}\tau + \mathbb{B}\dot{\tau} + \dot{\mathbb{Q}} - \ddot{x}_r) + \mu^T (\mathbb{A} + \mathbb{B}\tau + \mathbb{Q} - \ddot{x}_r) + \nu^T \dot{\tilde{x}} \quad (45)$$

According to sliding mode law, control input guarantees following condition on sliding surface convergence

$$\ddot{s} = -\rho s - \varrho \dot{s} - \sigma \tanh(K_{t1}s) - \varsigma \tanh(K_{t2}\dot{s}) \quad (46)$$

where  $\rho, \varrho, \sigma, K_{t1}$  and  $K_{t2}$  are positive definite matrices. Therefore, it can be deduced that as  $s \rightarrow 0$  then  $\tilde{x} \rightarrow 0$ . Rearranging above equation, control input is found to satisfy

$$\dot{\tau} = (\lambda^T \mathbb{A})^{-1} [-(\lambda^T \dot{\mathbb{B}} + \mu^T \mathbb{B})\tau - (\lambda^T \dot{\mathbb{A}} + \mu^T \mathbb{A}) - \nu^T \dot{\tilde{x}} - \rho s - \varrho \dot{s} - \sigma \tanh(K_{t1}s) - \varsigma \tanh(K_{t2}\dot{s}) + \lambda^T \ddot{x}_r + \mu^T \ddot{x}_r] \quad (47)$$

where  $\varsigma$  is subjected to the condition

$$\varsigma > \|\lambda^T \dot{\mathbb{Q}} + \mu^T \mathbb{Q}\|_\infty \quad (48)$$

Since  $B(x)$  is not invertible, its pseudo-inverse is employed below. As shown in Fig.3, the control input signal is represented as

$$\tau = (\lambda^T \dot{\mathbb{B}} + \mu^T \mathbb{B})^{-1} [-(\lambda^T \dot{\mathbb{A}} + \mu^T \mathbb{A} + \nu^T \dot{\tilde{x}}_r) - \rho s - \varrho \dot{s} - \sigma \tanh(K_{t1}s) - \varsigma \tanh(K_{t2}\dot{s}) + \lambda^T \ddot{x}_r + \mu^T \ddot{x}_r] [\exp -(\lambda^T \mathbb{B})^{-1} (\lambda^T \dot{\mathbb{B}} + \mu^T \mathbb{B}) t_c - 1] \quad (49)$$

For *HOSMC* law to show asymptotic stability, a function under direct *Lyapunov's* stability criterion is defined below for the sliding surface. It possesses a form of

$$V(t) = \frac{1}{2} \rho s^2 + \frac{1}{2} \dot{s}^2 + \sigma \ln(\cosh(K_{t1}s)) \quad (50)$$

The invariance property of *HOSM* is exploited to understand usefulness of the proposed policy. According to Lyapunov's direct law [14,18,21], the function  $V$  is differentiated w.r.t time  $t$  such that derivative of  $V$  exists and stays within bound

$$\dot{V}(t) = \dot{s}[-\rho s - \varsigma \tanh(K_{t2}\dot{s}) + \lambda^T \dot{\mathbb{Q}} + \mu^T \mathbb{Q}] < 0 \quad (51)$$

The experimental evaluation w.r.t control performance specifications further shows stability and ruggedness of proposed control strategy in real environment.

#### 4. EXPERIMENT RESULTS

The built spherical prototype shown in Fig.1 is a 3D printed on a precision multi-material *ProJet 5500X* printer.

Orientation and distance travelled is measured using InvenSense *MPU9150 IMU* and an encoder. It has a total mass (shell and cart) of 90 g with shell radius measuring 30 mm. Wheel mass and radius are calculated to be 0.19 g and 4.75 mm respectively. The *nRF* wireless module provides the robot communications. It is a fit for low power, long range and multi-agent applications. Robot control is done through the high speed data received from it. Two *Faulhaber 1512.003SR(30mNm/3V)* dc geardrive motors are used as actuators. Featured by low rotor inertia and metal commutation with integrated encoder, the motors provide precise rotor position. Proposed second-order sliding mode controller is computationally implemented by a 32 bit *ARM Cortex-M4* with a 10 KHz clockrate. Project design and implementation is done in *C++*. Wheel joint position and velocity response is calculated by an encoder fitted on each motor. Measured velocity values are differentiated to obtain joint acceleration. The derivative operation inherently behaves like a high pass-filter thereby adding noise to the data set noisy. A low-pass filter is used to attenuate noise in differentiated signal at the cost of incorporating a phase shift. Therefore, a loss of fidelity is observed. Rolling angles( $\beta$ ) generated from the rolling gait *CPG* (section 3.1) are fed to *HOSMC* feedback controller as reference. Resultant torque output  $\tau_c$  obtained from feedback  $\tau_{fb}$  (blue dotted line) path is applied to both wheel joints as shown in Fig.3. The controllers are responsible to regulate  $\beta, \dot{\beta}, \theta, \dot{\theta}$ . *IMU* senses  $\beta, \dot{\beta}$ . Angular position  $\theta_L, \theta_R$  and velocities  $\dot{\theta}_L, \dot{\theta}_R$  of drive wheels are recorded by encoders, which are used to calculate  $\theta, \dot{\theta}$ . Spherical robot control performance is compared for locomotion along a nonlinear trajectory. The trajectory is considered for both plane (indoor smooth) and irregular (outdoor rough) surfaces. Initial value of robot is taken at  $t = 0$  at its origin. Geared *DC* motors were actuated at 80 percent of maximum speed. Robot kinematics is used to convert resultant rolling gaits in both wheels to its translational motion. It comes with a time delay  $t_d$ . Assuming the control cycle to be  $t_c$ , the expected left and right wheel velocities after one control cycle are expressed as

$$\begin{aligned} \dot{\theta}_L &= \dot{\theta}(t + t_c + t_{1d}) - \dot{\varphi}(t + t_c + t_{2d}) \\ \dot{\theta}_R &= \dot{\theta}(t + t_c + t_{1d}) + \dot{\varphi}(t + t_c + t_{2d}) \end{aligned} \quad (52)$$

##### 4.1 Performance on Smooth Plane Surface (indoor)

The associated control torque input on system dynamics is illustrated in Fig.5(a) on a smooth plane surface, w.r.t both simulation and experimental stages. The rise times are comparable but a reduced steady state error is depicted by *HOSMC* compared to *SMC* sliding mode strategy. The figure later shows the corresponding settling pattern of both torques for desired rolling gaits. The roll angle behaviour ( $\beta$ ) of the robot motion on smooth surface is shown in Fig.5(b). The driving cart(wheel)on shell oscillates initially back and forth, before reducing to a stable margin of 0.32 rad during experiments. *HOSMC* shows less overshoot almost by a margin of 0.2 rad and less variation in steady state is seen in contrast to *SMC*. The angular velocity responses are illustrated in Fig.5(c) for left and right wheels. The velocities are measured as a reaction of robot (actuator) dynamics to the control torque. Both wheel velocities settle to a stable value

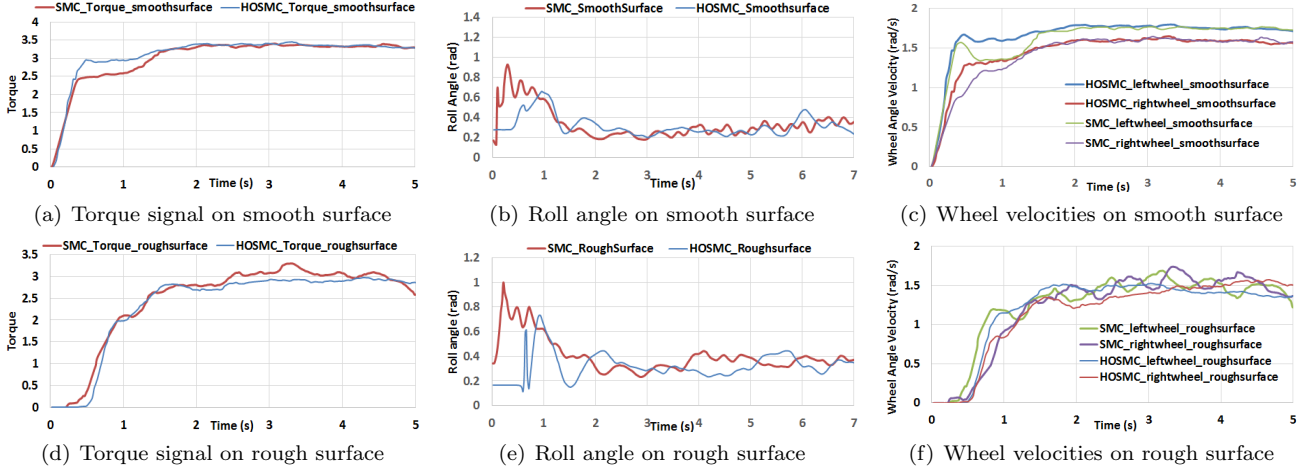


Fig. 5. Experiment and simulation results for smooth and rough surfaces

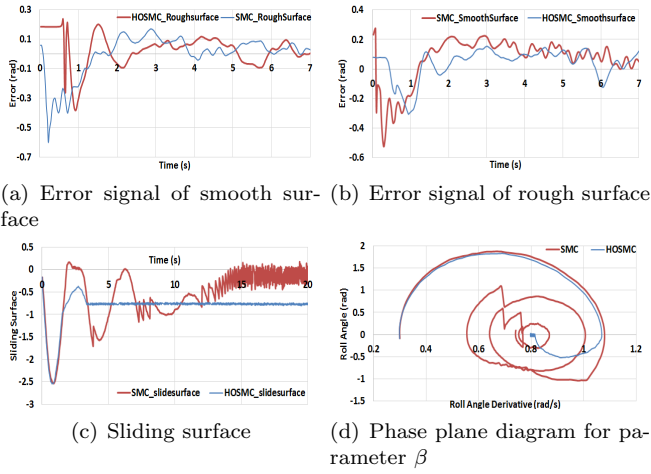


Fig. 6. CPG rolling gait and generated trajectory wrt parameter  $\beta$

before showing an improvement in minimum overshoot and steady state error in the case of *HOSMC*. It therefore results into a less jerky motion of the spherical robot. But from the same figure, it can be inferred that both wheels velocities deviate quite significantly from each other of 0.11 rad/s.

#### 4.2 Performance on Irregular Rough Surface (outdoor)

Successive set of experiments report the condition when the spherical robot platform is performing motion on uneven, irregular and rough surfaces. These surfaces are made of concrete with obtrusive deformations on it. The irregular surface alongside bounded external disturbances give rise to parameter uncertainties. The *HOSMC* control overcomes these issues better than the first-order *SMC* strategy. It is evident from the mild yet unstable oscillations of the later scheme while settling to a steady state, illustrated in Fig.5(d). The IMU sensor roll angle response of the robot motion is shown in Fig.5(e) for both schemes. It can be observed that *HOSMC* roll angle attains a higher (twice) overshoot with 0.72 rad on a rough surface compared to a lesser 0.61 rad on a smooth surface Fig.5(b). Compared to *SMC*, the proposed *HOSMC* shows reduced overshoot by margin of 0.28 rad.

The controlled roll angle signal settles down with more deviations observed in *SMC* than its counterpart. It also demonstrates the controller robustness in the presence of external disturbances and parametric uncertainties. The measured wheel angular velocity responses are shown in Fig.5(f). As expected of the surface deformations, they display less oscillatory behaviour in the case of *HOSMC* regulated within a stable boundary of 0.19 rad/s. Above results have also portrayed a small rise time and low error signal variation for the *HOSMC* compared to the *SMC* scheme, as seen in Fig.6(a) and 6(b). This leads to a more periodic variation in speed specifically with *SMC* scheme. During this period, it is also inferred consistency of both policies have to improve w.r.t robot dynamic model. Control gains need to be dynamically tuned to achieve better performance specifications. Fig.6(c) portrays the sliding surface of *HOSMC* and *SMC*. It can be observed that the sliding mode is in the longer reaching phase before arriving a sliding phase in the case of *SMC*. Illustrated in Fig.6(a) and(b), when the error is small, *HOSMC* surface variation is also very less compared to *SMC*. It is observed that corresponding sliding surface is non-zero, when the error signal has a finite value. In steady-state condition, the ideal sliding function behaviour is desired to be close to zero, but Fig.6(c) shows a practical situation in the presence of bounded disturbances, unmatched uncertainties and other nonlinearities discussed earlier. The phase plane diagram emanating from *HOSMC* and *SMC* based state trajectories is shown in Fig.6(d). It reveals a converging plot for the sustained stable oscillations for both. Compared to *SMC*, proposed *HOSMC* scheme shows smaller steady-state variations and faster convergence. It is found to closely reach the asymptotic equilibrium around a desired state ( $\beta$ ) trajectory region therefore resulting into a stable non-linear system transient response [14,18]. On the contrary, the *SMC* led state trajectory results in a longer path and time to dampen the oscillatory variations.

## 5. CONCLUSION

The manuscript presents the design and implementation of a second-order sliding mode control (*HOSMC*) of a CPG based spherical robot. The asymmetrical *CPG* model is inspired by the caterpillar-rolling gait. The resulting rolling gait acts as a trajectory generator. A comprehensive

dynamics model of spherical robot is presented comprising of actuator dynamics and rolling friction. A second-order sliding mode control is proposed to improve robustness performance of robot motion control system. Experiments are done to confirm the suitability of proposed spherical robot dynamics and *HOSMC* control strategy in both smooth (indoor environment) and rough irregular (outdoor environment) ground surfaces. The efficacy of the *HOSMC* controller is proven to show chattering attenuation, uncertainty handling capabilities and bounded disturbance rejection. Compared to the first-order sliding mode *SMC*, the proposed *HOSMC* controller shows performance improvement on closed-loop control design specifications. *HOSMC* provides a reduced error signal variation and faster asymptotic convergence of the roll ( $\beta$ ) state trajectory. The feasibility of a real-time spherical robot prototype propelled by mimicking an active rolling gait and *HOSMC* control architecture is demonstrated.

#### ACKNOWLEDGEMENTS

The authors gratefully acknowledge the support of the Temasek Lab @SUTD and the SUTD-MIT International Design Center. We would like to thank Mr. Akash Vibhute, Mr. Cheong Li Yang, Mr. Chen Xiohan for key contributions for the mechanical CAD and dynamics design of spherical robot. We would acknowledge useful suggestions and feedback given by Mr. Che Kun Law of Purdue University, Mr. Hu Yuan of Robotics Institute, Carnegie Mellon University and Mr. Peter Ho (Co-founder) of HOPE Technik Pte. Ltd.

#### REFERENCES

- [1] Armour R. H. and Vincent J. F. V. "Rolling in nature and robotics: a review". *J. Bionic Eng.*, vol. 3, pp. 195-208, 2006.
- [2] van Griethuijsen L.I. and Trimmer B.A. "Locomotion in caterpillars". *Biol. Rev.*, vol. 89, pp. 656-670, 2014.
- [3] Brackenbury J. "Fast locomotion in caterpillars". *J. Insect Physiol*, vol. 45, pp. 525-33, 1999.
- [4] Marder E and Bucher D "Central pattern generators and the control of rhythmic movements". *J. Insect Physiol*, vol. 11, pp. 986-996, 2001.
- [5] Ijspeert A. J. , "Central pattern generators for locomotion control in animals and robots: A review". *Neural Networks*, vol.21, pp. 642-653, 2008.
- [6] G. Li, H. Zhang, F. Herrero-Carrn, H. P. Hildre and J. Zhang, "Novel mechanism for caterpillar-like locomotion using asymmetric oscillation", *Proc. IEEE/ASME Int. Conf. Adv. Intell. Mech.*, pp. 164-169, 2011.
- [7] H.T. Lin, Gary G Leisk and Barry Trimmer "TGoQBot: a caterpillar-inspired soft-bodied rolling robot", *Bioinspir. Biomim.*, Vol. 6, pp. 026007, 2011.
- [8] C. P. Santos and V. Matos. "Gait transition and modulation in a quadruped robot: A brainstem-like modulation approach", *Robot. Auto. Syst.*, vol. 59, no. 9, pp. 620-634, 2011.
- [9] K. Matsuoka. "Sustained oscillations generated by mutually inhibiting neurons with adaptation", *Biol. Cybern.*, vol. 52, no. 6, pp. 367-376, 1985.
- [10] A. Bicchi, A. Balluchi D. Prattichizzo and A. Gorelli, "Introducing the Sphericle: An Experimental Testbed for Research and Teaching in Nonholonomy, Proceedings of the IEEE International Conference on Robotics and Automation, Albuquerque, NM, USA (1997) vol. 3, pp. 2620-2625.
- [11] S. Bhattacharya and S. Agrawal "Spherical Rolling Robot: A Design and Motion Planning Studies, *IEEE Transactions On Robotics And Automation*, 16(6), pp. 835-839, 2000.
- [12] E. Kayacan, Z. Y. Bayraktaroglu and W. Saeys "Modeling and control of a spherical rolling robot: A decoupled dynamics approach", *Robotica*, vol. 30, pp. 671-680, 2011.
- [13] Zhao, B. Li, M. Yu, H. Hu, H. Sun, L. "Dynamics and Motion Control of a Two Pendulums Driven Spherical Robot" *Proceedings of IEEE/RSJ International Conference on Intelligent Robots and Systems (IROS)*, Taipei, pp. 147-153, 2010.
- [14] V. I. Utkin "Sliding Modes in Control Optimization", Springer-Verlag, 1992.
- [15] P. Lamon and R. Siegwart "Wheel torque control in rough terrain-modeling and simulation", *Proceedings of the IEEE International Conference on Robotics and Automation Barcelona*, pp. 867-872, 2005.
- [16] Cai, Y., Zhan, Q., and Xi, X. "Path Tracking Control of a Spherical Mobile Robot. *Mechanism and Machine Theory*, Vol. 51, 58-73, 2011, 2012.
- [17] E. Kayacan, H. Ramon, and W. Saeys, "Adaptive neuro-fuzzy control of a spherical rolling robot using sliding-mode-control- theory-based online learning algorithm *IEEE Trans. Cybern.* , Vol. 43, no. 1, pp. 170-179, 2013.
- [18] M. Vidyasagar "Nonlinear Systems Analysis, Prentice Hall, NJ, 1993.
- [19] A. Borisov, A. Kilin, and I. Mamaev "How to control Chaplygin's sphere using rotors. Part II, *Regular and Chaotic Dynamics*, Vol. 18, no. 12, pp. 144-158, 2013.
- [20] A. Morinaga, M. Svinin, and M. Yamamoto "A motion planning strategy for a spherical rolling robot driven by two internal rotors, *IEEE Transactions on Robotics*, Vol. 30, no. 4, pp. 993-1002, 2014.
- [21] A. Levant, "Construction principles of 2-sliding mode design," *Automatica*, Vol. 43(4) , pp. 576-586, 2007.
- [22] F. Hamerlain, K. Achour, T. Floquet, W. Perruquetti, "Higher order sliding mode control of wheeled mobile robots in the presence of sliding effects," *44th IEEE Conference on Decision and Control and the European Control Conference*, pp. 1959-1963, 2005.
- [23] Abhra Roy Chowdhury, B. Prasad, V. Kumar, R. Kumar and S. K. Panda, "Bio-harmonized Dynamics Model for a Biology Inspired Carangiform Robotic Fish Underwater Vehicle", *19th IFAC World Congress*, Vol. 19, pp. 7258-7265, Capetown, 2014.
- [24] Abhra Roy Chowdhury and S. K. Panda "Finding Answers to Biological Control Methods using Modulated Patterns: An Application to Bio-inspired Robotic Fish". *IEEE International Conference on Robotics and Automation (ICRA)*, pp. 3146 - 3153. Seattle, USA, 2015.